Phys. Rev. A, submitted

Photoionization of Sc^{2+} ions by synchrotron radiation: High resolution measurements and absolute cross sections in the photon energy range 23–68 eV

S. Schippers,[1,*] A. Müller,[1] S. Ricz,[2] M. E. Bannister,[3] G. H. Dunn,[4] A. S. Schlachter,[5] G. Hinojosa,[6] C. Cisneros,[6] A. Aguilar,[7] A. M. Covington,[7] M. F. Gharaibeh,[7] and R. A. Phaneuf[7]

[1] *Institut für Kernphysik, Justus-Liebig-Universität, 35392 Giessen, Germany*[†]
[2] *Institute of Nuclear Research of the Hungarian Academy of Sciences (ATOMKI), H-4001 Debrecen, Hungary*
[3] *Physics Division, Oak Ridge National Laboratory, Oak Ridge, Tennessee 37831*
[4] *JILA, University of Colorado, Boulder, Colorado 80309-0440*
[5] *Lawrence Berkeley National Laboratory, Advanced Light Source, Berkeley, California 94720*
[6] *Centro de Ciencias Físicas, Universidad Nacional Autónoma de México, Apartado Postal 6-96, Cuernavaca 62131, Mexico*
[7] *Department of Physics, University of Nevada, Reno, Nevada 89557*[‡]

(Dated: September 30, 2002)

Cross sections for the photoionization (PI) of Sc^{2+} ions with [Ar]3d ground state configuration have been measured by employing the merged ion-photon beams method. The Sc^{2+} ions were produced from metallic vapor in an electron cyclotron resonance (ECR) ion source, and the photon beam was generated by an undulator in the electron-synchrotron storage-ring of the Advanced Light Source (ALS) of the the Lawrence Berkeley Laboratory. The experimental photon energy range 23–68 eV encompasses the direct 3d and 3p photoionization thresholds. The experimental photo-ion spectrum is dominated by autoionizing resonances due to 3p excitations predominantly decaying via Coster-Kronig and Super-Coster-Kronig transitions. Individual resonances located around $E \approx 40.2$ eV have been measured with an instrumental energy spread ΔE as low as 1.2 meV, corresponding to a resolving power of $E/(\Delta E)$ around 33 500. The fractions of metastable ions in the Sc^{2+} ion beam are obtained by comparing the photoionization cross section with the recently measured [Schippers et al, Phys. Rev. A **65**, 042723 (2002)] cross section for the time-reversed process of photorecombination (PR) of Sc^{3+} ions. Absolute strengths of several $3p^5 3d^2$ and $3p^5 3d\,4s$ PI resonances have been determined. They are the same as the corresponding resonance strengths for iso-electronic Ca^+ ions.

PACS numbers: 32.80.Fb, 32.80.Hd, 34.80Lx

I. INTRODUCTION

Doubly charged scandium with its [Ar]3d ground state configuration is the simplest atomic system with an open 3d shell [1]. It is even simpler than neutral scandium which, in addition, to the 3d electron, has a closed $4s^2$ shell outside the argon core. Therefore photoionization (PI) of Sc^{2+} is fundamentally interesting, especially in view of the severe discrepancies between experimental [2] and theoretical [3, 4] PI cross sections for neutral scandium in the region of $3p \rightarrow 3d$ excitations. Likewise, PI measurements with other, more complex transition metal atoms and ions [5, 6] revealed large deviations of the available theoretical results from the experimental ones. These discrepancies are due to the fact that an exact theoretical description of atomic systems with open 3p and 3d shells is extremely demanding and still beyond the capabilities of state-of-the-art atomic structure calculations. Nevertheless, because of the scarcity of experimental PI data for atomic ions, theoretically derived cross sections have to be relied upon, e. g., in the modeling of astrophysical or man-made plasmas. In response to this unsatisfying situation one of the objectives of the present study is to provide a benchmark for theoretical PI cross sections of complex ions.

Photoionization of Sc^{2+} via $3p \rightarrow 3d$ excitations can be represented as

$$\begin{array}{lcl} h\nu + Sc^{2+}(3s^2 3p^6 3d) & \rightarrow & Sc^{2+}(3s^2 3p^5 3d^2) \\ & \searrow & \downarrow \\ & & Sc^{3+}(3s^2 3p^6) + e^-. \end{array} \quad (1)$$

The vertical arrow represents the intermediate doubly excited $3p^5 3d^2$ states decaying predominantly by autoionization via Super-Coster-Kronig transitions, and the diagonal arrow represents the direct 3d PI channel. It is also possible to study the time reversed process of Eq. 1, i. e. the photorecombination (PR) of a $Sc^{3+}(3p^6)$ ion with a free electron (e^-). In PR the resonant and direct channels are termed dielectronic recombination (DR) and radiative recombination (RR), respectively.

Theoretically, on a state-to-state level, PI and PR cross sections are linked via the principle of detailed balance. In a preceding publication [7] we have used the principle of detailed balance to compare the present experimental Sc^{2+} PI cross sections with measured Sc^{3+} PR cross sections [8]. It was shown that the study of both processes

*Electronic mail: Stefan.E.Schippers@strz.uni-giessen.de
†Electronic address: http://www.strz.uni-giessen.de/~k3
‡Electronic address: http://www.physics.unr.edu/facility/pirf/pirf.html

yields complementary information about the doubly excited intermediate states involved. It can generally be expected that PR leads to the excitation of a larger number of resonances compared to PI where usually dipole selection rules limit the number of accessible intermediate states. Moreover, the final state of PR can also be an excited state (that eventually decays to the ground state of the recombined ion by the emission of one or several additional photons) while in a PI experiment one always starts from the ground state (and possibly from a few long-lived metastable states that might be present in an ion beam extracted from a hot plasma). The multitude of states involved in PR makes the experimental resolution and identification of individual DR resonances difficult. Complementary information from PI can help to identify individual PR pathways in this situation.

Correspondingly, a further motivation for the present study is to provide information about doubly excited Sc^{2+} states that is complementary to the results from a recent combined experimental and theoretical study of PR of Sc^{3+} by Schippers *e*t al. [8]. That PR work was motivated by the theoretical prediction [9] of an *asymmetric* line shape of the $3p^5 3d^2(^3F)\ ^2F$ DR resonance due to interference between the resonant and the direct PR channel. In the usual theoretical treatment of PR, e. g., for the production of PR rate coefficients for plasma physics applications, such interferences, quite commonly observed in PI, are neglected (independent processes approximation, IPA). They are considered to be relatively unimportant due to the existence of a multitude of competing, noninterfering recombination channels [10]. In the Sc^{3+} PR experiment of Schippers *et al.* [8] that was carried out to test the validity of the IPA, only weak evidence was found for an asymmetry of the $3p^5 3d^2(^3F)\ ^2F$ DR resonance, since the line-shape analysis was hampered by the limited experimental resolution and counting statistics. A Sc^{2+} PI experiment can be expected to yield more accurate information because of the much smaller experimental energy spread (due to the use of a photon beam instead of an electron beam) and because of a more favorable signal-to-noise ratio for ions with a low charge-to-mass ratio [8].

This paper is organized as follows. The experimental setup as well as the data acquisition and analysis procedures are described in Sec. II. In Sec. III we briefly describe atomic structure calculations performed to identify the most prominent resonances in the measured PI cross sections. The measured PI cross sections are presented in Sec. IV along with detailed spectroscopic information such as level energies, resonance widths and strengths extracted from the experimental data. Some resonances are identified with the aid of the atomic structure calculations from Sec. III. In Sec. V the present experimental PI data for Sc^{2+} are compared to the PR data for Sc^{3+} from Ref. [8]. In Ref. [7] we have already shown that this comparison yields the fractional abundances of metastable states in the Sc^{2+} ion beam, which was used in the present experiment, and thereby provides the experimental absolute Sc^{2+} PI cross-section scale. In Secs. VI and VII we compare our experimental results with a theoretical calculation of the Sc^{2+} PI cross section [11] and with measured PI resonance strengths of isoelectronic metastable $Ca^+(3p^6 3d)$ [12] and ground-state $Ca^+(3p^6 4s)$ [13] ions.

II. EXPERIMENT

We employed the merged photon-ion beams method [13, 14, 15, 16, 17, 18] for the measurement of photoionization cross sections. A schematic of the apparatus is shown in Fig. 1. The experiment was performed at the ion-photon beam (IPB) end station [19] of the undulator beamline 10.0.1 of the Advanced Light Source (ALS, Lawrence Berkeley National Laboratory). The beamline is capable of delivering photons with energies ranging from 17 to 340 eV with a flux of up to 5×10^{12} photons per second at 0.01% bandpass and a photon energy of 40 eV. After emerging from the undulator the photon beam passed through a monochromator equipped with three interchangeable reflection gratings. The low energy grating (380 lines/mm) covering photon energies up to 70 eV was used. As shown in Fig. 2 the photon energy spread can be adjusted in a nominal range from approximately 50 meV down to about 1.5 meV by changing the slit widths of the monochromator. The photon flux in the experiment was constantly monitored with a calibrated photodiode.

For the production of the Sc^{2+} ion beam, pieces of metallic scandium were vaporized in an electrically heated oven. The Sc^{2+} ion beam was generated by ionizing the scandium atomic vapor by electron bombardment inside a compact electron cyclotron resonance (ECR) ion source using exclusively permanent magnets for the confinement of the ECR plasma [20]. The ion beam was extracted by putting the ion source at a high voltage $U_{\rm acc} = +6$ kV with respect to the grounded ion beam transport system. After having traveled through a diploe bending magnet for selecting the desired ratio of charge to mass, the ion beam was centered onto the counterpropagating photon beam by applying appropriate voltages to several electrostatic ion-beam steering devices (see Fig. 1). A linear interaction region of well-defined length was created by putting a voltage $U_{\rm int} = +2$ kV on a cylindrical electrode of length $L = 29.4$ cm centered around the beam axis. Inside this "voltage labeled" region the ion beam energy was $E_{\rm ion} = eq(U_{\rm acc} - U_{\rm int}) = 8$ keV with e and q denoting the elementary charge and the ions' charge state, respectively.

Following the interaction zone the ion beam was deflected out of the photon beam direction by a second dipole magnet that also separated the ionized Sc^{3+} product ions from the Sc^{2+} parent ions. The Sc^{3+} ions were counted with nearly 100% efficiency with a single-particle detector, and the Sc^{2+} ion current was monitored for normalization purposes. The measured Sc^{3+} count rate R

was only partly due to photoionization events. It also contained Sc^{3+} ions produced by stripping collisions with residual gas molecules and surfaces as well as stray electrons and photons. This background was subtracted from the ionization signal by measuring the Sc^{3+} count rates $R^{(\mathrm{on})}$ and $R^{(\mathrm{off})}$ with the photon beam switched on and off, respectively. The photon beam was chopped with a frequency of 2 Hz and the data acquisition was gated accordingly.

For each selected photon energy $E_{h\nu}$ the photoionization cross section was evaluated as

$$\sigma(E_{h\nu}) = \frac{e^2 q\,\phi\,v_{\mathrm{ion}}}{I_{\mathrm{ion}} I_{h\nu}\,\eta\,L\,\Omega}\left[R^{(\mathrm{on})}(E_{h\nu}) - R^{(\mathrm{off})}(E_{h\nu})\right] \quad (2)$$

where $v_{\mathrm{ion}} = (2E_{\mathrm{ion}}/m_{\mathrm{ion}})^{1/2}$ denotes the ion velocity, $I_{h\nu}$ the electrical current given by the photodiode, ϕ the photodiode's sensitivity, and η the Sc^{3+} ion detection efficiency. The quantity Ω is the form factor describing the spatial overlap of the two beams. In principle, at our experimental setup a form-factor measurement can be achieved with a movable slit in the center of the voltage-labeled interaction region and with two wire scanners at each end of the interaction zone [19]. However, at the time of the present experiment, the rather low electrical ion currents of typically 3–4 nA prohibited the use of the wire scanners for a reliable beam overlap measurement. Therefore, in this work the absolute Sc^{2+} PI cross section scale was determined by applying the principle of detailed balance, i. e. by comparison of the present data with the measured absolute Sc^{3+} PR cross section from a storage-ring experiment [8] (see Ref. [7] and Sec. V below).

Energy scan measurements were taken by stepping the photon energy through a preset range of values. The mutually overlapping scans were limited to ranges of at most 3 eV. Each scan consisted of data at 300 equally spaced photon energies. At each energy, data were taken with the photon beam on and off as explained above. During the scan the monochromator settings and undulator gap were continuously adjusted such that the maximum photon flux was transmitted. Each scan was repeated as many times as needed to reach the desired level of statistical uncertainty.

Care was taken to calibrate the energy scale. First a Doppler correction was applied that takes the ions' motion into account. All nominal photon energies were multiplied by the Doppler correction factor $k_{\mathrm{D}} = [(c + v_{\mathrm{ion}})/(c - v_{\mathrm{ion}})]^{1/2}$ (here c denotes the speed of light) amounting to $k_{\mathrm{D}} = 1.000618317$ in the present case. Secondly, the Doppler-corrected energy scale was calibrated by adjusting separately measured threshold energies for the direct ionization of Ar^{+} and Ar^{2+} ions to the respective values taken from the NIST Atomic Spectra Database [21] using a linear transformation. In the energy range under study this calibration amounted to maximum energy changes of 60 meV. The error in the resulting calibrated energy scale is less than ±3 meV.

Because of the production of the ion beam from a hot ECR plasma it can be expected that considerable fractions of the Sc^{2+} ions are in the $3p^6 3d^2\ ^2D_{5/2}$ and $3p^6 4s\ ^2S_{1/2}$ metastable states with excitation energies [21] of 24.504 meV and 3.166473 eV above the $3p^6 3d^2\ ^2D_{3/2}$ ground state, respectively. Their calculated lifetimes [22] of about 1.2×10^4 s and 51 ms, respectively (cf., Table I), are both long enough for the survival of the metastable states during the ions' transport from the ion source to the interaction region with a flight time of the order of 10 μs. The measured cross section can only be put on an absolute scale when the composition of the ion beam is known. In Ref. [7] the fractional composition of the ion beam has already been determined by a comparison of the measured Sc^{2+} PI cross section with the experimental Sc^{3+} PR cross section of Schippers et al. [8]. The metastable fractions resulting from this comparison are listed in Table I, and further details of the procedure are given in Sec. V.

Systematic uncertainties of the absolute values for the Sc^{2+} photoionization cross section are estimated to be ±20%. This uncertainty is mainly due to the uncertainties associated with the determination of the metastable fractions in the Sc^{2+} ion beam and to the experimental uncertainty of the Sc^{3+} PR measurements [8].

III. ATOMIC STRUCTURE CALCULATIONS

In order to be able to identify at least the most prominent resonances in the measured Sc^{2+} PI cross section atomic structure calculations were performed using the codes of Cowan [23]. The accurate calculation of resonance energies, widths and strengths for atomic systems with open 3d shells is a challenging task. The highly correlated nature of the doubly excited $3p^5 3d^2$ states requires large basis set expansions as has been shown, e. g., by Hansen and Quinet [24] who performed calculations of $3p^6 3d \rightarrow 3p^5 3d^2$ transitions in metastable Ca^{+} ions. Although they considered the interaction between 10 initial and 16 final configurations, their calculated resonance positions are still 0.6 eV different than the experimental observations [12, 25]. When smaller basis sets are used, discrepancies between calculated and measured Sc^{2+} [8] and Ti^{3+} [26] $3p^5 3d^2$ resonance positions can be as large as ~ 3 eV.

In the present calculations we include for simplicity only $3p^6 3d$ and $3p^6 4s$ initial and $3p^5 3d^2$, $3p^5 3d\,4s$ and $3p^5 3d\,4d$ final configurations of Sc^{2+}. This set of configurations is by far too small for arriving at accurate transition energies and rates but should be sufficient to identify the strongest transitions. Following the prescription of Hansen and Quinet [24] we have scaled electrostatic integrals by a factor of 0.85 and left spin-orbit integrals unchanged. Resonance widths were calculated as $\Gamma = \hbar(\sum_r A_r + \sum_a A_a)$ where $\sum_r A_r$ and $\sum_a A_a$ denote the sums over all relevant radiative and autoionization rates, respectively. For the calculation of the latter, only transitions to the $Sc^{3+}(3p^6)$ ground state configuration were considered. We find that, except for some doubly

excited ^2D states, the widths of all resonances are essentially determined by the autoionization rates.

From our basis set we obtain 284 dipole allowed excitations ranging from about 24.5 to 57.5 eV. In Table II we only list those 33 transitions with weighted oscillator strengths $gf > 0.05$ and with resonance energies $E_{\rm res} < 43.2$ eV. Calculated transitions at higher energies are exclusively due to excitations to $3p^5 3d\,4d$ states. The PI resonance strength $\overline{\sigma}$ has been calculated as the product of the absorption strength and the branching ratio for autoionization, i. e.,

$$\overline{\sigma} = 4\pi^2 \alpha\, a_0^2\, \mathcal{R}\, \frac{gf}{g_i} \frac{\sum_a A_a}{\sum_r A_r + \sum_a A_a} \qquad (3)$$

with the fine structure constant α, the Bohr radius a_0, the Rydberg constant $\mathcal{R}$ and the statistical weight g_i of the initial state ($4\pi^2 \alpha\, a_0^2\, \mathcal{R} \approx 1.0976 \times 10^{-16}$ eV cm^2). The calculational results will be used in the following section for the identification of some of the resonances observed.

IV. RESULTS

An overview of the measured Sc^{2+} photoionization cross section extending over almost the entire experimental photon energy range is shown in Fig. 3; not shown is the energy range 63–68 eV, where as in the range 58–63 eV, no resonance structures have been detected within the statistical uncertainty. The broadest and strongest two resonances at 37.137 and 41.8065 eV (see Table II) are due to $3p^6 3d\ ^2D \rightarrow 3p^5 3d^2(^3F)\ ^2F$ and $3p^6 4s\ ^2S \rightarrow 3p^5 3d(^1P) 4s\ ^2P$ excitations, respectively. The appearance of the latter indicates that the ion beam contains a non-negligible fraction of Sc^{2+} ions in the $3p^5 3d(^1P) 4s\ ^2S_{1/2}$ metastable state.

Obviously the cross section for direct 3d photoionization of the $Sc^{2+}(3p^6 3d^2\ ^2D_{3/2})$ ground state is very small. No corresponding threshold at 24.75684 eV (Table I) is observed in Fig. 3. Likewise, the threshold for the direct 3d photoionization of the $^2D_{5/2}$ metastable states, that could be expected at 24.73234 eV is not observed. The threshold of the $3p^6 4s\ ^2S_{1/2}$ metastable state at 21.59037 eV is in the energy region where the efficiency of the monochromator's reflection grating drops sharply and its measurement therefore has not been attempted. Although no direct ionization threshold is discernible in our data, the direct PI channel manifests itself by interference with resonant channels leading to asymmetric line shapes of the associated resonances. This is exemplified in Fig. 4 that zooms in on the energy region 29.5–33.0 eV. All four observed resonances can be fitted by an asymmetric Fano profile [27, 28]

$$F(E) = \frac{A}{Q^2 \Gamma} \frac{2}{\pi} \left[\frac{(Q+\varepsilon)^2}{1+\varepsilon^2} - 1 \right] \qquad (4)$$

with $\varepsilon = 2(E–E_{\rm res})/\Gamma$, the resonance energy $E_{\rm res}$, the resonance width Γ, and the asymmetry parameter Q. The term -1 inside the square brackets ensures that $F(E) \rightarrow 0$ for $E \rightarrow \pm\infty$. Low values of $|Q|$ correspond to a high degree of asymmetry. In the limit $Q \rightarrow \infty$ the Fano profile as defined by Eq. 4 approaches the symmetric Lorentzian line profile

$$L(E) = \frac{A}{\Gamma} \frac{2}{\pi} \frac{1}{1+\varepsilon^2} \qquad (5)$$

with the peak area A. For the fit shown in Fig. 4 the individual Fano profiles have been convoluted with a normalized Gaussian to represent the experimental energy resolution (see Ref. [8] for computational details). For $Q \rightarrow \infty$ this convolution yields a Voigt line profile. The convolution introduces the experimental energy spread ΔE, i. e., the Gaussian full width at half maximum (FWHM), as a further fit parameter. From the fits we find that the fitted energy spread is always somewhat lower than the nominal energy spread as derived from the monochromator settings.

The fitted Q-values for the first and second pairs of resonances shown in Fig. 4 are 10 ± 17 and 6.8 ± 1.4, respectively. Especially in the second pair the asymmetry is clearly visible. In the fit we have somewhat arbitrarily assumed the same Q value for each of the two pairs of resonances. Also fitted was a constant background level of $5.3 \pm 0.5 \times 10^{-19}$ cm^2 representing the contribution of the nonresonant direct PI channel averaged over the energy interval of Fig. 4. The fitted resonance widths are rather large. The fit yields $\Gamma \approx 0.14$ eV for the first two resonances (in the fit the same width was used for both resonances) and $\Gamma \approx 0.11$ eV for the third and fourth resonances. These large widths suggest that the main decay channel of the resonances is a fast autoionizing Super-Coster-Kronig $3p^5 3d^2 \rightarrow 3p^6$ transition. According to our atomic structure calculations (Table II) the strongest transitions in the energy interval of Fig. 4 are to states of ^2F symmetry belonging to the $3p^5 3d^2$ configuration. While the calculated resonance energies of 30.29, 30.40, 31.43 and 31.82 eV are too high by about 0.2 eV, the relative peak positions almost correspond to the experimental findings. The calculated and fitted widths agree with each other to within 50%. A similar agreement between theory and experiment is found for the next two groups of resonances at higher energies due to $3p^6 3d\ ^2D \rightarrow 3p^5 3d^2(^3P)\ ^2P$ excitations (Fig. 5a) and to $3p^6 3d\ ^2D \rightarrow 3p^5 3d^2(^3F)\ ^2F$ excitations (Fig. 5b). Using the tabulated (Table I, see Ref. [7] and below) relative abundances of metastable states in the Sc^{2+} ion beam, the fitted peak areas can be converted into absolute resonance strengths. These are of the same order of magnitude as the theoretical values.

The resonances in the energy range 35.9-36.9 eV cannot be identified on the basis of our atomic structure calculations. The Roman numerals labeling the peaks shown in Figs. 6 and 7 (measured with higher resolution than the spectrum displayed in Fig. 3) also appear in Table II where we summarize the results of the Voigt line profile fits to the measured resonances. The strongest cal-

culated excitations in this energy range are of the type 3p → 4s leading from $3p^6 3d\ ^2D$ to $3p^5 3d 4s\ ^2D$ and ^2F doubly excited states of relatively small calculated widths. Except for the resonances XI and XIV the measured widths are one to two orders of magnitude larger than calculated. The reason for the small widths of the ^2D states is easily understood in therms of pure LS coupling by the fact that parity and angular momentum conservation rules forbid the autoionizing decay of pure $3p^5 3d\,nl\ ^2D$ states of odd parity to the $3p^6\ ^1S_{1/2}$ final state. The decay of the ^2D states becomes possible only because of the admixture of, e. g., ^2P or ^2F states by relativistic effects. The degree of mixing in the calculation does not seem to be sufficient to explain the observed resonance widths.

Figure 8 shows the giant $3p^6 3d\ ^2D \rightarrow 3p^5 3d^2(^3F)\ ^2F$ resonance at 37.137 eV. Clearly, its line shape is asymmetric by interference with the direct 3d photoionization channel. The fitted asymmetry parameter $Q = 5.02 \pm 0.08$ is smaller than those of the other broad $3p^5 3d^2\ ^2F$ resonances displayed in Fig. 4. The calculated position and width of the giant resonance are 37.93 eV and 1.06 eV, respectively. The measured resonance energy is 0.86 eV lower than the calculated one. The calculated width is 25% larger than the fitted width of 0.847 ± 0.005 eV. It is interesting to note that the same value (within the experimental errors), i. e., 0.89 ± 0.07 for the resonance width was extracted from PR measurements with Sc^{3+} ions [8]. Because of the large width the fine structure of the resonance cannot be resolved.

The fine-structure splitting between the $3p^6 3d^2\ ^2D_{3/2}$ ground state and the $3p^6 3d^2\ ^2D_{5/2}$ metastable state can be inferred from their excitations to the $3p^5 3d^2(^3P)\ ^2P_{3/2}$ (Fig. 9) and $3p^5 3d^2(^3F)\ ^2D_{5/2}$ states (Fig. 10). The experimental energy difference between the $^2D_{5/2} \rightarrow ^2P_{3/2}$ and the $^2D_{3/2} \rightarrow ^2P_{3/2}$ resonances amounts to 24.8 ± 0.3 meV. Exactly the same difference is found between the $^2D_{5/2} \rightarrow ^2D_{5/2}$ and $^2D_{3/2} \rightarrow ^2D_{5/2}$ resonances. It should be noted that the deviation of our value for the $Sc^{2+}(3p^6 3d\ ^2D)$ fine structure splitting from the value 24.504 meV given in the NIST atomic spectra database is within our experimental uncertainty.

The measured $^2D \rightarrow ^2P$ resonance positions (Fig. 9) are ∼ 0.61 eV lower than the calculated ones. The calculated resonance widths range from 2.64 to 2.67 meV. These values are relatively close to the experimental ones that range from 2.3 to 4.6 meV. The theoretical resonance strengths are factors of 2–3 larger than the experimental ones. The resonance labeled XVI in Fig. 9 cannot be assigned to any of the calculated transitions. Fig. 10 contains two unidentified resonances labeled XVII and XVIII. As shown in the inset of Fig. 10 the resonance XVII could only be resolved when the highest experimental resolution was used corresponding to a resolving power of $E/\Delta E \approx 33\,500$!

The $^2D \rightarrow ^2D$ resonances in Fig. 10 have been identified on the basis of the fine-structure splitting of the ground state as mentioned above. Measured and theoretical ^2D resonance positions differ by ∼0.77 eV. The calculated widths are factors of about 4 lower than the ones obtained from the Voigt line profile fits to the measured resonances. This latter discrepancy is again attributed to deficiencies in the accurate calculation of relativistic effects that are most important for the ^2D doubly excited states. The calculated Auger decay rate of the $3p^5 3d^2(^3F)\ ^2D_{3/2}$ is 5 orders of magnitude lower than that of the $3p^5 3d^2(^3F)\ ^2D_{5/2}$ state. Correspondingly, the branching ratio for Auger decay of the $^2D_{3/2}$ state is very small (3.2×10^{-6}), and the calculated associated resonance strengths (Eq. 3) are negligible. Therefore, no measured peaks are assigned to $3p^6 3d\ ^2D \rightarrow 3p^5 3d^2(^3F)\ ^2D_{3/2}$ excitations. According to our calculation, the fine structure splitting of the doubly excited $3p^5 3d^2(^3F)\ ^2D$ states is almost the same as the fine structure splitting of the $3p^6 3d\ ^2D$ initial states. This is another reason why resonance XVIII cannot be identified with the $3p^6 3d\ ^2D_{3/2} \rightarrow 3p^5 3d^2(^3F)\ ^2D_{3/2}$ transition. Its distance of 34.9 meV from the neighboring $3p^6 3d\ ^2D_{3/2} \rightarrow 3p^5 3d^2(^3F)\ ^2D_{5/2}$ resonance is larger than the ^2D fine structure splitting of 24.8 ± 0.3 meV.

The last resonance that could be identified on the basis of our atomic structure calculations is the strong $3p^6 4s\ ^2S_{1/2} \rightarrow 3p^5 3d(^1P)4s\ ^2P$ resonance formed at 41.087 eV. Its calculated width is nearly 50% larger than its experimental width of 0.148 eV and its calculated position of 43.19 eV is 1.38 eV higher than the experimental value. This fits the trend of an increasing discrepancy between measured and calculated resonance positions with increasing resonance energy. For the lowest $^2D \rightarrow ^2F$ resonances around 31 eV the discrepancy is ∼ 0.25 eV, for the $^2D \rightarrow ^2P$ resonances around 39.7 eV it is ∼ 0.61 eV, and for the $^2D \rightarrow ^2D$ resonances around 40.2 eV it amounts to 0.77 eV. The discrepancy is probably due to the neglect of interaction with higher excited configurations in our calculations. This neglect introduces larger errors for the more highly excited states.

The identification of individual resonances out of the multitude of PI resonances observed above 43 eV (Fig. 3) is prohibitive. According to our atomic structure calculations, transitions to $3p^5 3d\,4d$ states cover the energy range 43-57.5 eV. In principle $3p \rightarrow ns$ and $3p \rightarrow nd$ excitations with $n \geq 5$ can also lead to resonances up to the highest threshold for direct $3p$ ionization at 67.53 eV[21]. In the PR cross section of Sc^{3+}, Rydberg series of $3p^5 3d(^1P)\,nl$ and $3p^5 4s(^1P)\,nl$ DR resonances have been observed [8]. In the present PI study no such Rydberg series are evident.

V. COMPARISON WITH PR MEASUREMENTS

The principle of detailed balance relates the cross section $\sigma^{(\mathrm{PI})}(h\nu)$ for PI to the cross section $\sigma^{(\mathrm{PR})}(E_{\mathrm{cm}})$ for PR on a state-to-state level. Accordingly, for nonrela-

tivistic photon energies $h\nu \ll m_e c^2$

$$\sigma_{f\to i}^{(\mathrm{PR})}(E_{\mathrm{cm}}) = \frac{(h\nu)^2}{2m_e c^2\, E_{\mathrm{cm}}} \frac{g_i}{g_f}\, \sigma_{i\to f}^{(\mathrm{PI})}(h\nu) \qquad (6)$$

where i denotes the initial state — Sc^{2+} ion + photon of energy $h\nu$ — and f denotes the final state — Sc^{3+} ion + electron with energy E_{cm} in the electron-ion center-of-mass (c. m.) frame [29]. The quantities g_i and g_f are the statistical weights of the ionic initial and final states, respectively. Here the statistical weight of the $3p^6\ ^1S_0$ state is $g_f = 1$ and the statistical weights g_i are listed in Table I. As shown in Fig. 11 the energy of the photon is given as the sum of the ionization potential I_i of the Sc^{2+} ion in state i and the energy of the free electron:

$$h\nu = I_i + E_{\mathrm{cm}}. \qquad (7)$$

The ionization potentials relevant to the present study are also listed in Table I.

When comparing PI and PR cross sections on the basis of Eq. 6, one generally has to be aware of the fact that the number of PR channels starting from state f is usually much larger than the number of PI channels ending in state f (cf. Fig. 11). Total recombination cross sections, that are usually measured in merged-beams electron-ion recombination experiments [30, 31], can therefore not be directly compared to photoionization cross sections unless the relative strengths for the various radiative decay channels are known.

However the situation is quite favorable here especially for the $3p^5 3d^2$ configuration, since it can safely be assumed, that the radiative transition to the $3p^6 3d\ ^2D$ ground state (vertical thick full arrow in Fig. 11) by far dominates all other transitions to excited $3p^6\, nl$ states (vertical thin full arrows in Fig. 11). The relative strength for the $3d \to 3p$ transition is practically unity. This is even also the case for the decay of $3p^5 3d\, 4s$ states, where in principle $4s \to 3p$ transitions can also be expected to form strong recombination channels. From our atomic structure calculations we find, however, that, e. g., for the strong $3p^5 3d(^1P)4s\ ^2P$ resonance, the $4s \to 3p$ radiative rates are two to three orders of magnitude smaller than the $3d \to 3p$ radiative rates. In this respect, Sc^{2+} is thus a very special ion with a true one-to-one correspondence between PI and PR via low-lying doubly excited states.

Having established that the relative strengths of the radiative decay paths of the resonances listed in Table II are unity, we can construct partial recombination cross sections $\sigma_{f\to i}^{(\mathrm{PR})_i}$ for the three separate recombination channels that populate each of the three initial PI states i. By inserting the experimental PI cross section data [with the PI resonance energies shifted by I_i (see Table I and Eq. 7)] into Eq. 6, each entry in Table II yields a PR resonance. Partial PR cross sections are obtained by carrying out appropriate summations over all doubly excited states d that can be reached from a given initial state i. Of course we can include only those resonances that have been identified with the aid of the atomic structure calculations. Thus we represent the cross section for PR by

$$\sigma_{f\to i}^{(\mathrm{PR})_i}(E_{\mathrm{cm}}) = \frac{1}{\eta_i} \frac{g_i}{g_f} \frac{(E_{\mathrm{cm}} + I_i)^2}{2m_e c^2\, E_{\mathrm{cm}}} \sum_d L_{i\to d}(E_{\mathrm{cm}}). \qquad (8)$$

The resonance line profile $L_{i\to d}(E_{\mathrm{cm}})$ is either a Lorentzian (Eq. 5) or Fano profile (Eq. 4), as appropriate, and η_i denotes the fractional abundance of state i in the Sc^{2+} ion beam of the PI experiment.

As shown in Fig. 12 the fractional abundances of the $3p^6 3d^2\ ^2D_{3/2}$ ground and the $3p^6 3d^2\ ^2D_{5/2}$, and $3p^6 4s\ ^2S_{1/2}$ metastable states, in the following denoted by $\eta_{3/2}$, $\eta_{5/2}$, and $\eta_{1/2}$ respectively, can be obtained from fitting the sum of the three partial DR cross sections to the measured PR cross section of Schippers *et al.* [8]. From the fit, where the condition $\eta_{3/2} + \eta_{5/2} + \eta_{1/2} = 1$ was imposed, we obtain $\eta_{3/2} = 0.237 \pm 0.011$, $\eta_{5/2} = 0.503 \pm 0.007$, and $\eta_{1/2} = 0.260 \pm 0.009$. In order to be able to include the broad $3p^5 3d^2(^3F)\ ^2F$ resonance with its unresolved fine structure in the fit it has been assumed on the basis of our atomic structure calculations that the cross section for its excitation is the same for both ^2D initial states. In order to check whether this assumption influences the fit results, we also performed a fit without including the $3p^5 3d^2(^3F)\ ^2F$ resonance. The fitted fractions η_i changed only marginally. It should be noted that, in addition to the fractional abundances, the absolute PI cross-section scale was also obtained from the fit by introducing an overall factor as an additional fit parameter.

Another parameter that was varied during the fit was an energy offset allowing for matching the PR and the PI energy scales. Matching of the scales can be achieved by shifting the PR energy scale by only 0.13 eV towards higher energies. This value is within the experimental uncertainty of the PR energy scale [8].

Apart from yielding the composition of the ion beam, the PI-PR-comparison in principle is also capable of assigning an initial state to each unidentified resonance labeled with Roman numerals in Table II. This is achieved by including the unidentified resonances in the partial cross sections such that the χ^2 of the fit to the measured PR spectrum is minimized. The best fit is shown in Fig. 13. Compared to the fit shown in Fig. 12 it yields slightly different fractions $\eta_{3/2} = 0.177 \pm 0.011$, $\eta_{5/2} = 0.590 \pm 0.007$, and $\eta_{1/2} = 0.233 \pm 0.009$ and a somewhat lower overall scaling factor of 0.35 ± 0.01. According to the fit, all unidentified resonances start either from the $^2D_{3/2}$ state — resonances I–IX, XI, XVII, and XVIII — or from the $^2D_{5/2}$ state — resonances X, XII–XIV, and XVI — apart from resonance XV at 39.262 eV that starts from the $^2S_{1/2}$ initial state. This latter designation is unambiguous since the inclusion of this resonance in either ^2D partial cross section would lead to a distinct peak at ~ 14.7 eV in the PR spectrum that was not measured. The initial state designations of the

other unidentified resonances are less certain. The question whether a given resonance belongs to the $^2D_{3/2}$ or to the $^2D_{5/2}$ initial state cannot always unambiguously be answered from the fit. The uncertainties of the η_i values given in Table I partly reflect the change of η_i when the unidentified resonances are distributed in different ways among the three partial PR cross sections. It should be noted that, apart from the fractional abundances, the absolute PI cross section scale was also obtained from the same fit as another fit parameter.

The overall agreement between the measured and the fitted PR spectrum (Fig. 13) is excellent, apart from some unreproduced PR resonance strength around 10 eV. It may be speculated that this unaccounted PR resonance strength stems from transitions between higher excited states that were not included in the partial spectra. The good agreement strongly supports the underlying assumption that all relative strengths for the radiative transitions from the doubly excited resonance states to the respective PI ground states are unity.

The same value of $\sim$ 0.85 eV for the width of the $3p^5 3d^2(^3F)\ ^2F$ resonance has been obtained from both the PI and the PR experiments. Within the experimental uncertainties, the PR asymmetry parameter $Q = 6.3 \pm 1.8$ agrees with the PI value $Q = 5.02 \pm 0.08$ (Table II). On the basis of R-matrix calculations, Schippers *et al.* [8] have speculated that besides the interference between nonresonant and resonant processes, the interference between adjacent resonances of the same symmetry could also be partly responsible for the observed asymmetry. The experimental resolution of the PR experiment was too low to be able to provide a test of this hypothesis. In the present high-resolution PI cross sections, we do not observe any of the predicted [8] signs of resonance-resonance interference.

VI. COMPARISON WITH OTHER THEORY

The photoionization of Sc^{2+} ions has recently been treated theoretically by Altun and Manson [11] who used many-body perturbation theory (MBPT). The theoretical result is compared with our measured Sc^{2+} PI cross section in Fig. 14. The theoretical curve exhibits significantly less resonance structure than the experimental curve. This is due to the fact that the calculations have been performed under *LS*-coupling conditions. Consequently, fine-structure splittings are not resolved and resonances generated by relativistic effects such as the $3p^5 3d^2\ ^2D$ resonances as discussed in Sec. IV are not calculated. Moreover, resonances that are excited from the $3p^6 4s\ ^2S_{1/2}$ metastable state, such as the ones at 39.2624 and 41.8065 eV in the experimental cross section (Table II), have not been considered by the theory.

It is obvious that the theoretical result deviates significantly from the experimental findings. In the theoretical spectrum the $3p^5 3d^2$ resonances are more spread out than in the experimental spectrum. The lowest member of this group is the $3p^5 3d^2(^1G)\ ^2F$ resonance. Its calculated position at 29.54 eV is $\sim$ 0.5 eV *lower* than the experimental value of 30.03 eV for the larger fine-structure component. The highest member of the $3p^5 3d^2$ group is the $3p^5 3d^2(^3F)\ ^2D$ resonance that theoretically does not exist within the *LS*-coupling approximation. For the one but highest $3p^5 3d^2(^3P)\ ^2P$ resonance the theoretical position at 41.57 eV is $\sim$ 1.8 eV *higher* than the experimental position of 39.69 eV. The theoretical position of the giant $3p^5 3d^2(^3F)\ ^2F$ resonance at 40.50 eV appears to be shifted by even 3.86 eV towards higher energies.

Not only the resonance positions but also the theoretical resonance strengths differ considerably from the experimental ones [32]. The calculated strength of the $3p^5 3d^2(^1G)\ ^2F$ resonance is almost an order of magnitude larger than the experimental value. The calculated strengths of the $3p^5 3d^2(^3P)\ ^2P$ and $3p^5 3d^2(^3F)\ ^2F$ resonances are higher than the experimental values by about factors of 2 and 1.5, respectively. On the other hand no experimental evidence is found for a strong $3p^5 3d^2(^1D)\ ^2P$ resonance which is predicted by theory at 29.75 eV.

These discrepancies are symptomatic of the general difficulty to describe atomic systems with open $3p$ and $3d$ shells correctly. It should be noted, however, that rather satisfactory agreement between experiment and theory is obtained for the width of the broad $3p^5 3d^2(^3F)\ ^2F$ resonance, i. e., 0.91 eV (theoretical) vs. 0.85 eV (experimental). Also the theoretical asymmetry parameter of 6.2 for this resonance is reasonably close to the experimental asymmetry parameter of 5.0.

VII. COMPARISON WITH ISO-ELECTRONIC CALCIUM

Kjeldsen et al. [12] have recently measured absolute cross sections for PI of metastable $Ca^+(3p^6 3d)$ ions. Although the experimental energy spread in those measurements was too large to resolve individual resonances on the fine-structure level it is instructive to compare the measured $Ca^+(3p^5 3d^2)$ resonance strengths with the corresponding values for Sc^{2+}. For the most prominent $3p^5 3d^2(^3F)\ ^2F$, $3p^5 3d^2(^3F)\ ^2D$ and $3p^5 3d^2(^3P)\ ^2P$ resonances in Ca^+ Kjeldsen et al. obtained 5.20×10^{-17}, 2.14×10^{-17}, and 2.23×10^{-17} eV cm^2, respectively. Within the experimental uncertainty our corresponding Sc^{2+} values are 6.3×10^{-17}, 2.9×10^{-17}, and 2.1×10^{-17} eV cm^2 (cf. Table II), consisten with the Ca^+ values.

Furthermore, our value of 2.3×10^{-16} eV cm^2 for the $3p^5 3d(^1P)\, 4s\ ^2P$ resonance due to the excitation of metastable $Sc^{2+}(3p^6\, 4s)$ ions can also be compared with the corresponding value 2.5×10^{-16} eV cm^2 obtained from PI measurements with Ca^+ ions in the $3p^6\, 4s\ ^2S$ ground state [13]. Again both values agree with one another.

The fact that these coincide underlines the validity of our novel method for the purely experimental derivation

of absolute state-selective PI cross sections by combining the high resolving power of a PI experiment at a synchrotron light source with the state selectivity of a heavy-ion storage-ring PR experiment.

VIII. CONCLUSIONS AND OUTLOOK

The present experimental investigation of the PI of Sc^{2+} ions is among the first studies on multiply charged transition metal ions using the merged-beams method. Due to the high photon flux available at the ALS PI cross sections could be measured with low statistical uncertainty even at relatively low ion densities. Detailed spectroscopic information on $3p \rightarrow 3d$ resonances could be obtained. This opens up promising prospects for further studies with more highly charged ions.

Sc^{2+} is the prototype of an atomic system with an open $3d$ shell. Its relatively simple ground-state configuration consists of a closed argon core with just one additional $3d$ electron. Despite that expected simplicity the theoretical description of the PI of Sc^{2+} appears to be very challenging. Recent state-of-the-art theoretical calculations are largely at odds with the present experimental findings. Individual resonance positions are off by more than 3 eV, and theoretical resonance strengths differ by up to an order of magnitude. order of magnitude. This may be due in part to relativistic effects that play an important role in the atomic structure of Sc^{2+} but were not included in the theoretical treatment. For the accurate description of PI resonances in strongly correlated many-electron systems atomic structure theory will need further development.

One problem with multiply charged ion beams extracted from a hot plasma is the existence of an usually unknown fraction of metastable ions in the beam. Here the metastable fractions were determined by a comparison between experimental PI and PR cross sections that employs the principle of detailed balance. Moreover, the comparison clarified some previously unresolved questions in the Sc^{3+} PR work of Schippers *et al.* [8] related to the occurrence of interference effects in PR cross sections.

Acknowledgments

We thank Z. Altun for providing the calculated Sc^{2+} PI cross section in numerical form. We gratefully acknowledge financial support through the Deutsche Forschungsgemeinschaft (MU 1068/10, A.M., S.S.), through NATO Collaborative Research Grants CRG-950911 (A.M., S.S.), CLG-976362 (S.R.), and from the Division of Chemical Sciences, Biosciences and Geosciences of the U.S. Department of Energy under contract DE-FG03-97ER14787 (A.A., A.M.C., M.F.G., R.A.P.). G.H.D. was supported in part by US DOE contract DE-A102-95ER54293, and M.E.B. was supported in part by the Office of Fusion Energy Sciences of the US DOE under contract DE-AC05-00OR22725 with UT-Battelle, LLC. A.A. acknowledges a fellowship granted by DGAPA-UNAM.

[1] The ground state configuration of both neutral potassium and singly charged calcium is [Ar]$4s$.
[2] S. B. Whitfield, K. Kehoe, R. Wehlitz, M. O. Krause, and C. D. Caldwell, Phys. Rev. A **64**, 022701 (2001).
[3] Z. Altun and S. T. Manson, Phys. Rev. A **59**, 3576 (1999).
[4] M. Martins, J. Phys. B. **35**, L223 (2002).
[5] B. Sonntag and P. Zimmermann, Rep. Prog. Phys. **55**, 911 (1992).
[6] H. Kjeldsen, B. Kristensen, F. Folkmann, and T. Andersen, J. Phys. B **35**, 3655 (2002).
[7] S. Schippers, A. Müller, S. Ricz, M. E. Bannister, G. H. Dunn, J. Bozek, A. S. Schlachter, G. Hinojosa, C. Cisneros, A. Aguilar, A. Covington, M. F. Gharaibeh, and R. A. Phaneuf, Phys. Rev. Lett. (in print).
[8] S. Schippers, S. Kieslich, A. Müller, G. Gwinner, M. Schnell, A. Wolf, A. Covington, M. E. Bannister, and L. B. Zhao, Phys. Rev. A **65**, 042723 (2002).
[9] T. W. Gorczyca, M. S. Pindzola, F. Robicheaux, and N. R. Badnell, Phys. Rev. A **56**, 4742 (1997).
[10] M. S. Pindzola, N. R. Badnell, and D. C. Griffin, Phys. Rev. A **46**, 5725 (1992).
[11] Z. Altun and S. T. Manson, J. Phys. B **32**, L255 (1999).
[12] H. Kjeldsen, F. Folkmann, F. Innocenti, L. Zuin, and J. E. Hansen, J. Phys. B **35**, L375 (2002).
[13] I. C. Lyon, B. Peart, K. Dolder, and J. B. West, J. Phys. B **20**, 1471 (1987).
[14] M. Oura, S. Kravis, T. Koizumi, Y. Itoh, T. Kojima, M. Sano, T. Sekioka, M. Kimura, K. Okuno, and Y. Awaya, Nucl. Instrum. Methods B **86**, 190 (1994).
[15] F. Wuilleumier, J.-M. Bizau, D. Cubaynes, B. Rouvellou, and L. Journel, Nucl. Instrum. Methods B **87**, 190 (1994).
[16] H. Kjeldsen, F. Folkmann, H. Knudsen, M. S. Rasmussen, J. B. West, and T. Andersen, J.Phys. B **32**, 4457 (1999).
[17] J. B. West, J. Phys. B **34**, R45 (2001).
[18] A. M. Covington, A. Aguilar, I. R. Covington, M. Gharaibeh, C. A. Shirley, R. A. Phaneuf, I. Álvarez, C. Cisneros, G. Hinojosa, J. D. Bozek, I. Dominguez, M. M. Sant'Anna, A. S. Schlachter, N. Berrah, S. N. Nahar, and, B. M. McLaughlin, Phys. Rev. Lett. **87**, 243002 (2001).
[19] A. M. Covington, A. Aguilar, I. R. Covington, M. F. Gharaibeh, G. Hinojosa, C. A. Shirley, R. A. Phaneuf, I. Alvarez, C. Cisneros, I. Dominguez-Lopez, A. S. Schlachter, N. Berrah, B. M. McLaughlin, and, A. Dalgarno, (2002), to be published.
[20] F. Brötz, R. Trassl, R. W. McCullough, W. Arnold, and E. Salzborn, Phys. Scr. **T92**, 278 (2001).

[21] W. C. Martin, J. Sugar, A. Musgrove, W. L. Wiese, J. R. Fuhr, D. E. Kelleher, K. Olsen, P. J. Mohr, G. Dalton, M. Douma, R. Dragoset, S. Kotochigova, L. Podobedova, E. Saloman, C. Sansonetti, and, G. Wiersma, *NIST Atomic Spectra Data Base*, National Institute of Standards and Technology, Gaithersburg, Maryland 20899-3460, USA, 2nd ed. (1999), `http://physics.nist.gov/cgi-bin/AtData/main_asd`.

[22] C. J. Zeippen, Astron. Astrophys. **229**, 248 (1990).

[23] R. D. Cowan, *The Theory of Atomic Structure and Spectra* (University of California Press, Berkeley, 1981).

[24] J. E. Hansen and P. Quinet, J. Elec. Spectros. Rel. Phenom. **79**, 307 (1996).

[25] A. Müller, S. Schippers, A. M. Covington, A. Aguilar, G. Hinojosa, R. A. Phaneuf, M. M. SantAnna, A. S. Schlachter, J. D. Bozek, and C. Cisneros, in *XXII International Conference on Photonic, Electronic, and Atomic Collisions, Santa Fe, New Mexico, USA, July 18-24, 2001, Abstracts of Contributed Papers*, edited by S. Datz, M. E. Bannister, H. F. Krause, L. H. Saddiq, D. Schultz, and C. R. Vane (Rinton Press, Princeton, New Jersey, 2001), p. 52.

[26] S. Schippers, T. Bartsch, C. Brandau, G. Gwinner, J. Linkemann, A. Müller, A. A. Saghiri, and A. Wolf, J. Phys. B **31**, 4873 (1998).

[27] U. Fano, Phys. Rev. **124**, 1866 (1961).

[28] U. Fano and J. W. Cooper, Phys. Rev. **137**, A1364 (1965).

[29] M. R. Flannery, in *Atomic, Molecular & Optical Physics Handbook*, edited by G. W. Drake (AIP Press, Woodbury, New York, 1996), pp. 605–629.

[30] A. Müller and A. Wolf, in *Accelerator-based atomic physics techniques and applications*, edited by J. C. Austin and S. M. Shafroth (AIP Press, Woodbury, 1997), p. 147.

[31] A. Müller and S. Schippers, in *Spectroscopy Challenge of Photoionized Plasmas*, edited by G. Ferland and D. W. Savin (Astronomical Society of the Pacific, San Francisco, USA, 2001), vol. 247 of *ASP Conference Proceedings*, pp. 53–78.

[32] Theoretical resonance positions were taken from Table 2 of Ref. [11]. Theoretical values for resonance strenghts, widths and asymmetry parameters were obtained by fitting Fano line profiles to the calculated resonance line shapes.

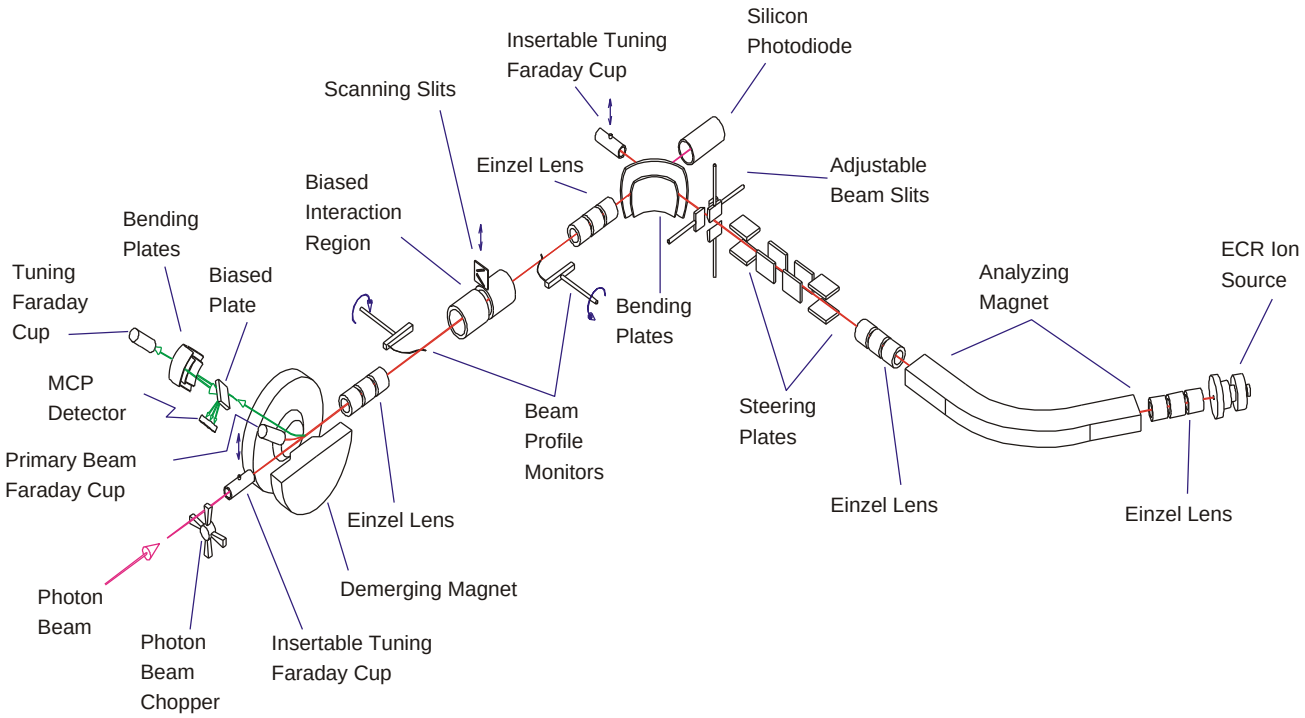

FIG. 1: Schematic of the ion-photon beam (IPB) end station at beamline 10.0.1 of the Advanced Light Source (ALS).

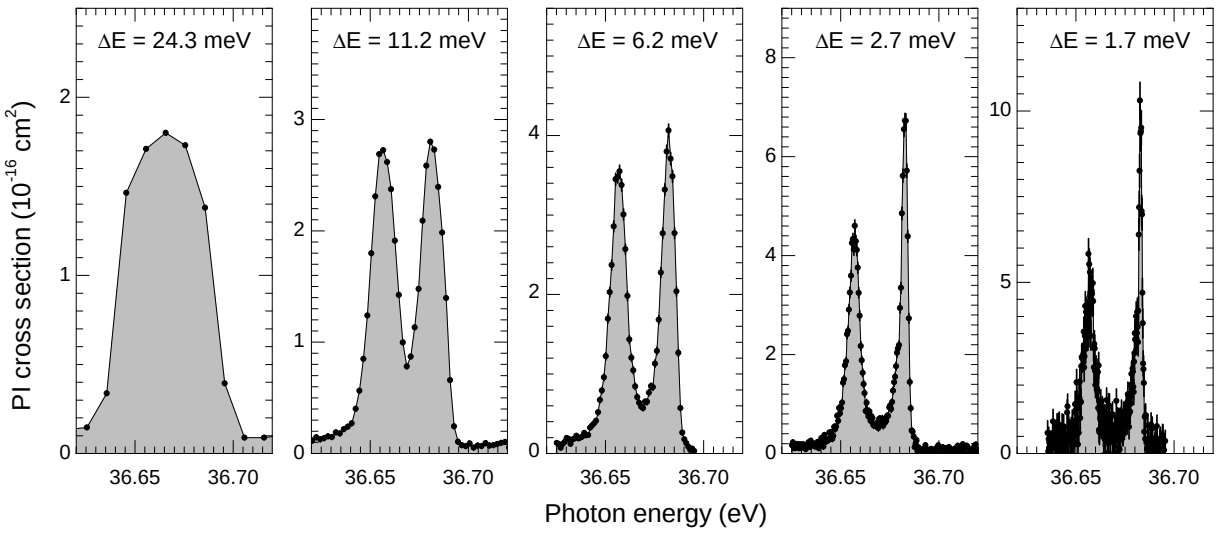

FIG. 2: Influence of the experimental resolution on the measured photoionization cross section for a group of 3 resonances located around 36.67 eV. The given experimental energy spreads have been determined from fits of Voigt line profiles to the measured resonance peaks. Note that the cross section scale increases when going from low to high resolution.

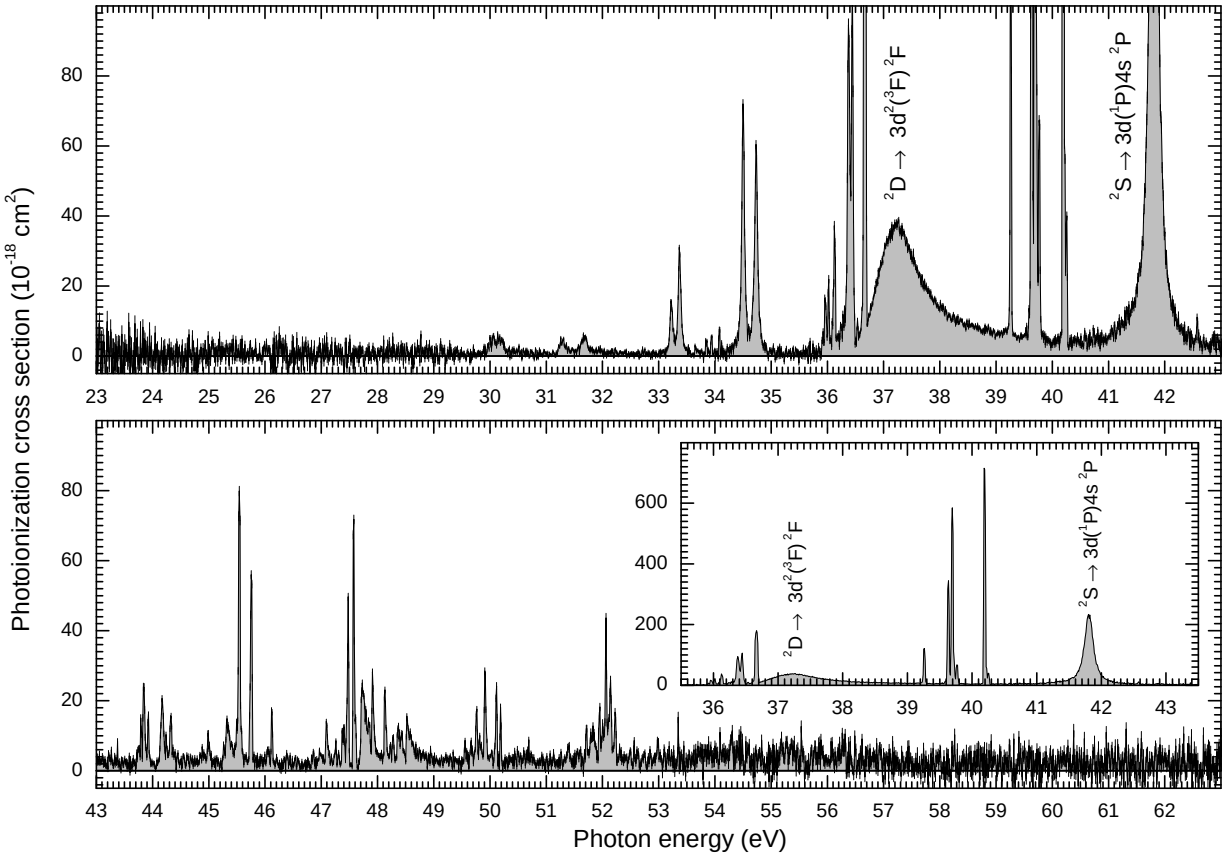

FIG. 3: Overview over the Sc^{2+} photoionization cross section measured with a nominal experimental energy spread of $\Delta E =$ 40 meV. The energy range 63–68 eV is not shown, since it does not contain any visible resonances. The broad resonances at 37.137 and 41.8065 eV (see Table II) are attributed to $3p^6 3d\ ^2D \rightarrow 3p^5 3d^2(^3F)\ ^2F$ and $3p^6 4s\ ^2S \rightarrow 3p^5 3d(^1P)4s\ ^2P$ excitations, respectively. The inset shows the full magnitudes of the strong resonances in the energy range 35.5–43.5 eV.

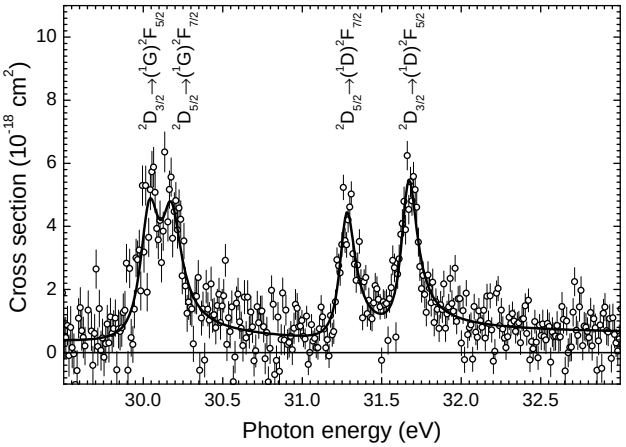

FIG. 4: Expanded view of the lowest-energy group of measured resonances associated with $3p^6 3d\ ^2D \rightarrow 3p^5 3d^2\ ^2F$ excitations. The resonances exhibit asymmetric line shapes which can be fitted by Fano profiles convoluted with a Gaussian. The results of the fit (full line) are contained in Table II. In the fit the experimental energy spread was kept fixed at $\Delta E = 19$ meV.

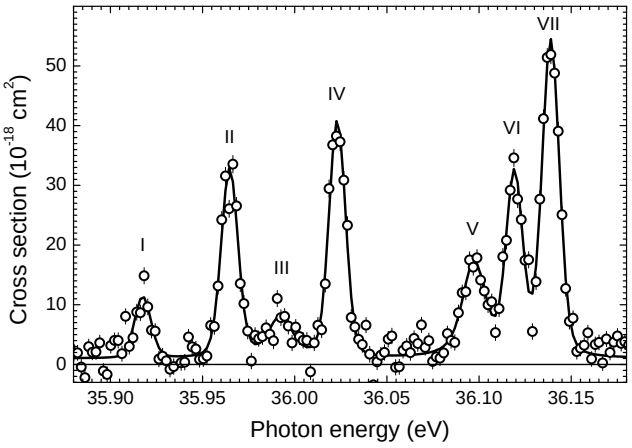

FIG. 6: Voigt line profile fits (full lines) to measured PI resonances (open symbols) in the photon energy range 35.88–36.18 eV. The fitted experimental energy spread is $\Delta E = 9.7 \pm 0.5$ meV. Further fit results are summarized in Table II where the resonances can be identified with the aid of the Roman numerals shown.

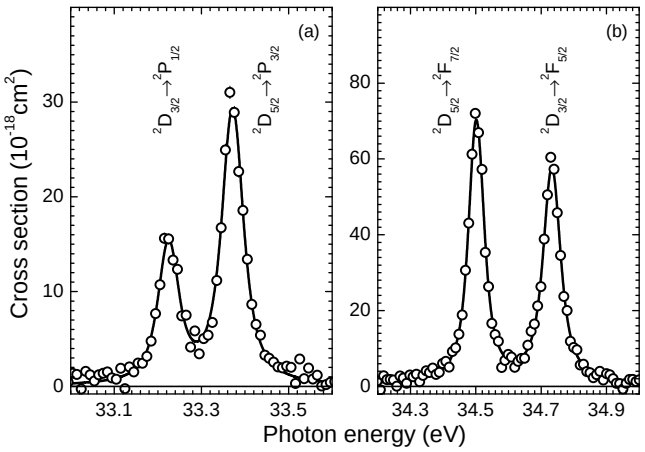

FIG. 5: Fits to the measured resonances due to $3p^6 3d\ ^2D \rightarrow 3p^5 3d(^3P)4s\ ^2P$ excitations (a) and $3p^6 3d\ ^2D \rightarrow 3p^5 3d(^3F)4s\ ^2F$ excitations (b) using Voigt line profiles. The experimental energy spreads obtained from the fits are $\Delta E = 22 \pm 3$ meV (a) and $\Delta E = 22 \pm 2$ meV (b). Further results of the fits (full lines) are contained in Table II.

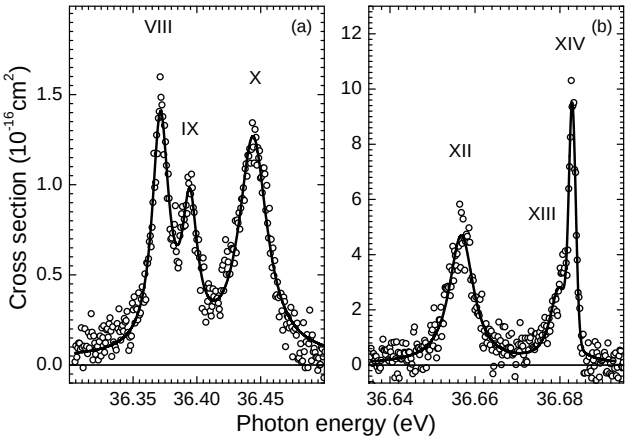

FIG. 7: Voigt line profile fits (full lines) to high resolution measurements (open symbols) in the photon energy ranges 36.3–36.5 eV (a) and 36.635–36.695 eV (b). From the fit (a) the experimental energy spread $\Delta E = 1.87 \pm 0.08$ meV is obtained. The same value has been used and kept fixed in fit (b). Further fit results are summarized in Table II where the resonances are labeled by Roman numerals.

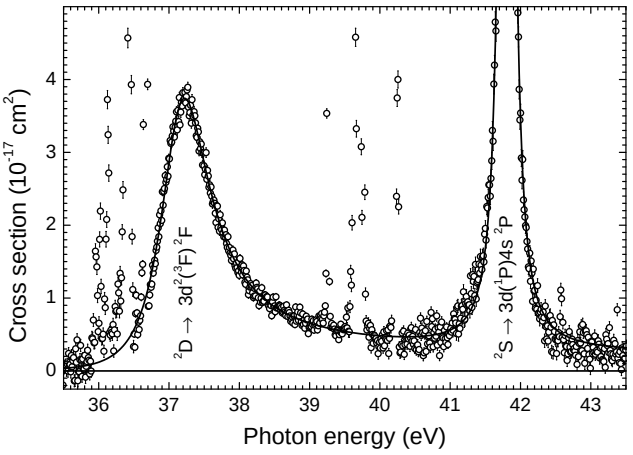

FIG. 8: Convoluted Fano profile and Voigt fit (full line) to the broad $3p^5 3d^2(^3F)\ ^2F$ and $3p^5 3d\,(^1P)4s\ ^2P$ resonances at 37.137 and 41.8065 eV, respectively. Due the large natural widths of these resonances of 0.847 and 0.148 meV, respectively, their fine structure splitting cannot be resolved. The $3p^5 3d^2(^3F)\ ^2F$ resonance exhibits a pronounced asymmetry. Its asymmetry parameter as obtained from the fit is 5.02 ± 0.08 (see also Table II). The energy range of the fit was 35.5–43.5 eV. Narrow resonances in this range were individually excluded from the fit. The fitted experimental energy spread is $\Delta E = 44 \pm 4$ meV.

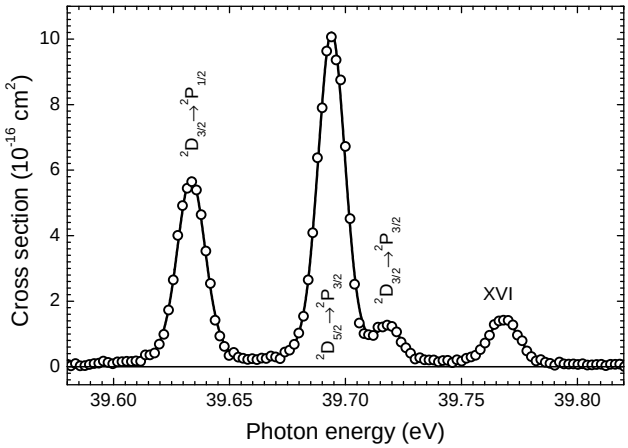

FIG. 9: Measured (open symbols) and fitted (full line) photoionization cross section in the region of the $3p^6 3d\ ^2D \rightarrow 3p^5 3d^2(^3P)\ ^2P$ resonances. The fitted experimental energy spread is $\Delta E = 11.6 \pm 0.1$ meV. Further results of the fits are contained in Table II. The experimental energy difference of 24.8 ± 0.3 meV between the $^2D_{5/2} \rightarrow {}^2P_{3/2}$ and the $^2D_{3/2} \rightarrow {}^2P_{3/2}$ resonances corresponds to the fine structure splitting of the $Sc^{2+}(3p^6 3d\ ^2D)$ state.

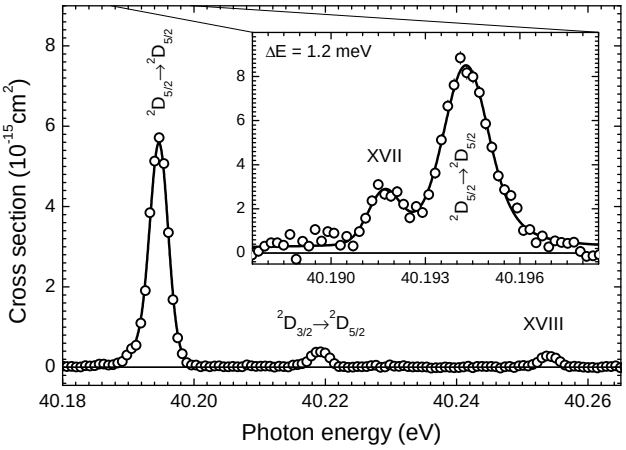

FIG. 10: Measured (open symbols) and fitted (full line) photoionization cross section in the region of the $3p^6 3d\ ^2D \rightarrow 3p^5 3d^2(^3F)\ ^2D$ resonances measured with high resolution. From the fits of Voigt profiles to the measured resonances $\Delta E = 2.88 \pm 0.04$ meV is obtained and $\Delta E = 1.20 \pm 0.09$ meV, respectively. The latter value corresponds to a resolving power $E/\Delta E$ of 33 500. The inset reveals that the peak at 40.195 eV is composed of at least two resonances. Further results of the fits are contained in Table II. Here, as in Fig. 9 the experimental energy difference of 24.8 ± 0.3 meV between the $^2D_{5/2} \rightarrow {}^2D_{5/2}$ and the $^2D_{3/2} \rightarrow {}^2D_{5/2}$ resonances corresponds to the fine structure splitting of the $Sc^{2+}(3p^6 3d\ ^2D)$ state.

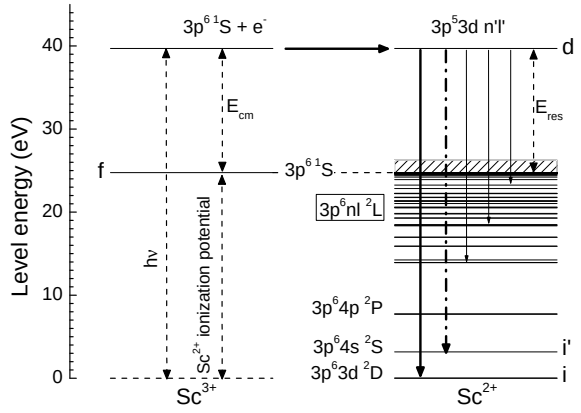

FIG. 11: Energy level diagram (level energies taken from Ref. [21]) for the dielectronic (resonant) recombination of Sc^{3+} ions. The initial state is composed of the ion in the $3p^6\,{}^1S$ ground state and a free electron with energy $E_{\rm cm}$ above the first Sc^{2+} ionization threshold. If $E_{\rm cm} \approx E_{\rm res}$ a $Sc^{2+}(3p^5 3d\,nl')$ doubly excited state may be formed by dielectronic capture (inverse autoionization) with nonzero probability (horizontal full arrow). The recombination event is completed by a subsequent radiative transition to a bound state below the Sc^{2+} ionization threshold. Generally, radiative transitions are possible not only to the $Sc^{2+}(3p^6 3d\ {}^2D)$ ground state (vertical thick full arrow) but also to an infinite number of $Sc^{2+}(3p^6 nl')$ excited states of appropriate symmetry (vertical thin full arrows). On the scale of the figure fine-structure level splittings are not resolved.

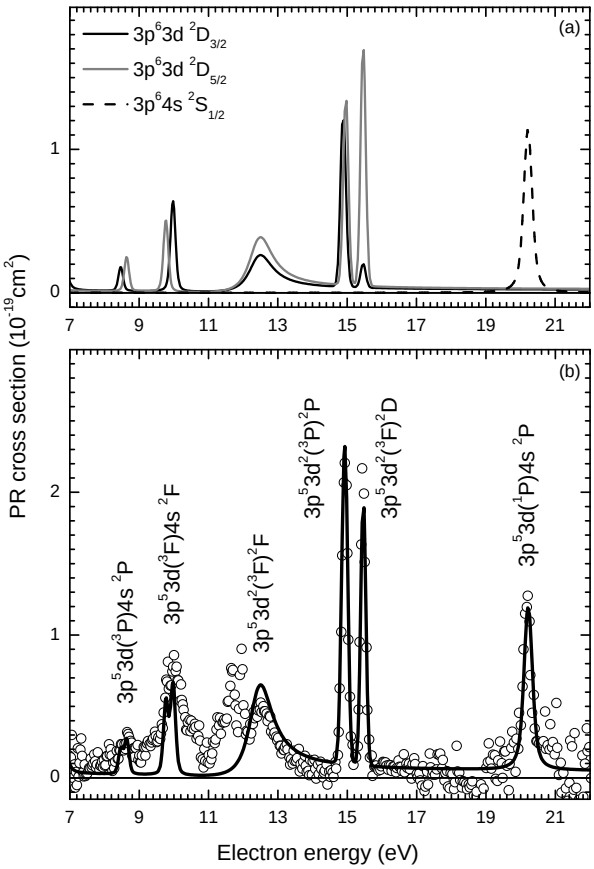

FIG. 12: Fit of the weighted sum of partial PR cross sections derived from the present PI measurements to the experimental PR cross section of Ref. [8]. In order to match the experimental PI and PR energy scales the PR energy scale ($E_{\rm cm}$) was shifted within its experimental uncertainty by 0.13 eV towards higher energies. The resonance line shapes were convoluted with a Gaussian representing the resolution of the Sc^{3+} PR experiment. In the fit only those PI resonances were used that could be identified on the basis of our atomic structure calculations (cf. Table II). The partial cross sections $\sigma^{({\rm PR})_i}$ (cf. Eq. 8) adding up to the total fit result [full line in (b)] are shown separately in (a).

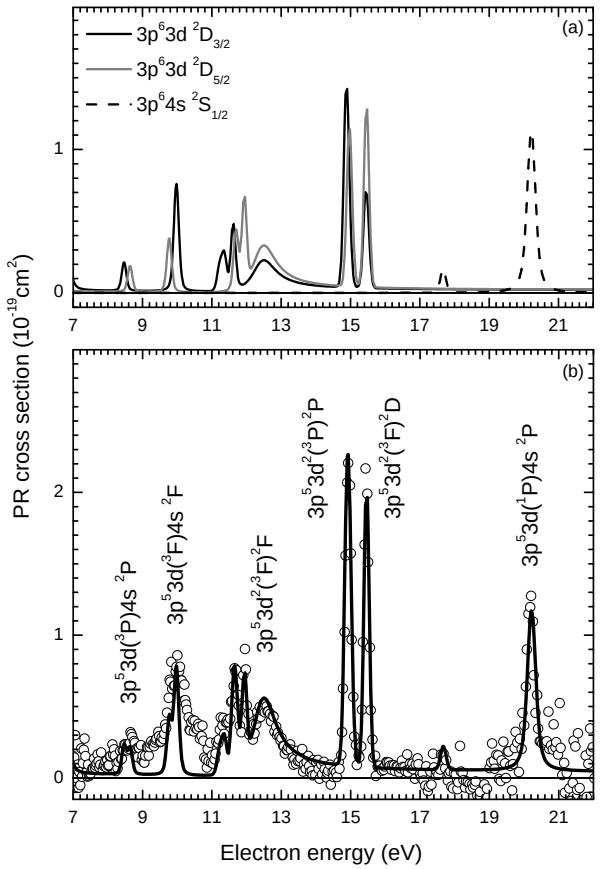

FIG. 13: Fit similar to that in Fig. 12 (circle points), but with the unidentified peaks (labeled with Roman numerals in Table II) included (see text).

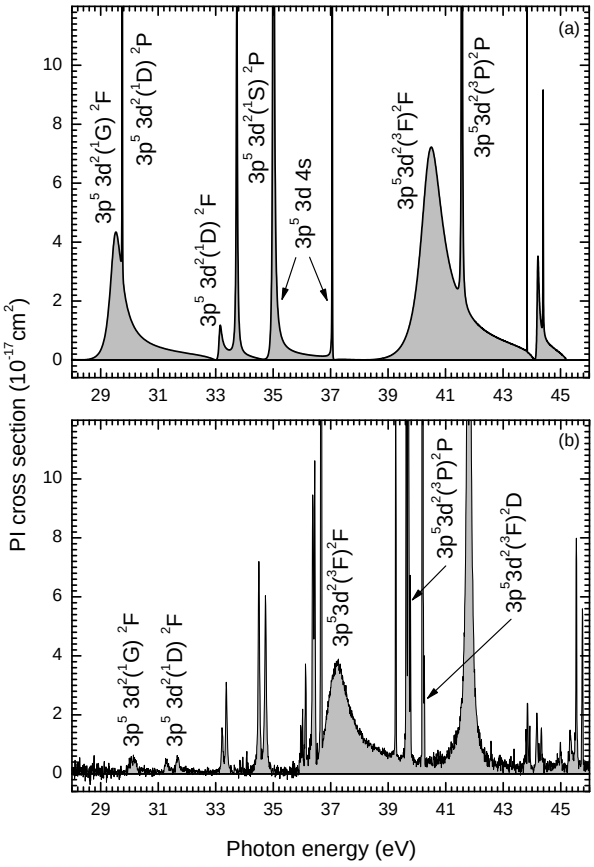

FIG. 14: Comparison of the measured Sc^{2+} photoionization cross section (b) with the MBPT cross-section calculation by Altun and Manson (a) [11].

TABLE I: Statistical weights g_i, ionization potentials I_i (from Ref. [21]) and lifetimes τ_i (from Ref. [22]) of the Sc^{2+} ground state and of the first two excited, metastable states. The fractions η_i of each state in the Sc^{2+} ion beam have been determined by comparing measured PI and PR cross sections (see Ref. [7] and Sec. V).

state		g_i	I_i (eV)	τ_i (s)	η_i (%)
$3p^6 3d$	$^2D_{3/2}$	4	24.75684	∞	20.7±3.0
$3p^6 3d$	$^2D_{5/2}$	6	24.73234	1.20×10^4	54.6±5.0
$3p^6 4s$	$^2S_{1/2}$	2	21.59037	0.0514	24.7±2.0

TABLE II: Theoretical and experimental resonance energies $E_{\rm res}$, widths Γ, resonance strengths $\overline{\sigma}$, peak areas A and asymmetry parameters Q. Only calculated transitions with weighted oscillator strengths $gf > 0.05$ and with $E_{\rm res} < 43.2$ eV are listed. The experimentally observed resonances labeled with Roman numerals cannot be identified on the basis of our calculations. However, in case of resonance XV the initial state could unambiguously be identified as the $^2S_{1/2}$ metastable state. The given errors of the experimental resonance strengths are the quadrature sums of the uncertainties of the measured peak areas and of the errors in the fractional abundances as listed in Table I. Additionally, the experimental resonance strengths possess an overall systematic error of ±15%. The systematic error of the experimental energy scale is less than ±3 meV.

Theory					Experiment				
$E_{\rm res}$ (eV)	gf	Γ (meV)	$\overline{\sigma}$ (10^{-18} eV cm^2)	Transition [a]	$E_{\rm res}$ (eV)	Γ (meV)	A (10^{-18} eV cm^2)	$\overline{\sigma}$	Q
30.29	0.084	110.	2.31	$^2D_{3/2} \rightarrow 3d^2(^1G)\ ^2F_{5/2}$	30.03(2)	142.(32)	0.9(3)	4.4(16)	10.(17)
30.40	0.114	113.	2.08	$^2D_{5/2} \rightarrow 3d^2(^1G)\ ^2F_{7/2}$	30.17(2)	142.(32)	0.7(2)	1.3(4)	10.(17)
31.43	0.149	107.	2.73	$^2D_{5/2} \rightarrow 3d^2(^1D)\ ^2F_{7/2}$	31.274(4)	111.(9)	0.72(5)	1.3(1)	6.8(14)
31.82	0.114	121.	3.13	$^2D_{3/2} \rightarrow 3d^2(^1D)\ ^2F_{5/2}$	31.663(4)	116.(8)	0.87(5)	4.2(7)	6.8(14)
33.22	0.234	33.1	6.41	$^2D_{3/2} \rightarrow 3d(^3P)4s\ ^2P_{1/2}$	33.2244(6)	45.(2)	1.22(3)	5.9(9)	
33.35	0.379	28.4	6.93	$^2D_{5/2} \rightarrow 3d(^3P)4s\ ^2P_{3/2}$	33.3716(4)	48.(2)	2.52(4)	4.6(4)	
34.36	1.180	36.9	21.6	$^2D_{5/2} \rightarrow 3d(^3F)4s\ ^2F_{7/2}$	34.5018(3)	44.(1)	5.71(7)	10.5(8)	
34.56	0.060	37.9	1.09	$^2D_{5/2} \rightarrow 3d(^3F)4s\ ^2F_{5/2}$					
34.59	0.981	37.9	26.9	$^2D_{3/2} \rightarrow 3d(^3F)4s\ ^2F_{5/2}$	34.7329(3)	53.(1)	5.39(7)	26.(4)	
				I	35.9175(4)	1.5(14)	0.12(1)		
				II	35.9647(2)	1.9(8)	0.36(2)		
				III	35.9923(9)	9.3(30)	0.14(2)		
				IV	36.0231(2)	1.6(7)	0.47(2)		
				V	36.0973(4)	8.7(13)	0.32(2)		
				VI	36.1191(2)	1.6(10)	0.36(2)		
				VII	36.1389(2)	2.5(6)	0.69(2)		
				VIII	36.3714(2)	15.3(6)	3.1(1)		
				IX	36.3945(3)	13.8(10)	1.6(9)		
				X	36.4440(2)	26.5(8)	5.0(1)		
				XI	36.5404(6)	$< 0.1(-)$	0.096(8)		
				XII	36.6568(9)	6.3(3)	4.9(2)		
				XIII	36.6799(3)	4.4(5)	2.1(2)		
				XIV	36.6829(2)	$< 0.1(-)$	1.7(1)		
36.13	0.126	0.189	2.28	$^2D_{5/2} \rightarrow 3d(^1D)4s\ ^2D_{5/2}$					
36.14	0.293	0.125	7.85	$^2D_{3/2} \rightarrow 3d(^1D)4s\ ^2D_{3/2}$					
36.16	0.073	0.189	2.00	$^2D_{3/2} \rightarrow 3d(^1D)4s\ ^2D_{5/2}$					
36.26	0.402	0.325	7.28	$^2D_{5/2} \rightarrow 3d(^1F)4s\ ^2F_{5/2}$					
36.28	0.087	0.325	2.36	$^2D_{3/2} \rightarrow 3d(^1F)4s\ ^2F_{5/2}$					
36.33	0.520	0.082	9.22	$^2D_{5/2} \rightarrow 3d(^1F)4s\ ^2F_{7/2}$					
36.55	0.815	0.440	14.7	$^2D_{5/2} \rightarrow 3d(^3D)4s\ ^2D_{5/2}$					
36.57	0.088	0.019	1.09	$^2D_{5/2} \rightarrow 3d(^3D)4s\ ^2D_{3/2}$					
36.58	0.166	0.440	4.50	$^2D_{3/2} \rightarrow 3d(^3D)4s\ ^2D_{5/2}$					
36.60	0.540	0.019	10.0	$^2D_{3/2} \rightarrow 3d(^3D)4s\ ^2D_{3/2}$					
37.90	0.343	1060.	6.27	$^2D_{5/2} \rightarrow 3d^2(^3F)\ ^2F_{5/2}$					
37.93	5.62	1060.	154.	$^2D_{3/2} \rightarrow 3d^2(^3F)\ ^2F_{5/2}$ }	37.137(3)	847.(5)	47.6(3)	63.(3)	5.02(8)
38.06	7.99	1070.	146.	$^2D_{5/2} \rightarrow 3d^2(^3F)\ ^2F_{7/2}$					
				XV	39.2624(2)	6.0(2)	4.59(5)	18.6(10)	
40.26	2.73	2.64	74.8	$^2D_{3/2} \rightarrow 3d^2(^3P)\ ^2P_{1/2}$	39.6335(2)	4.6(1)	10.09(5)	49.(2)	
40.30	4.93	2.67	90.3	$^2D_{5/2} \rightarrow 3d^2(^3P)\ ^2P_{3/2}$	39.6940(2)	3.8(1)	16.97(7)	31.(2)	
40.32	0.476	2.67	13.1	$^2D_{3/2} \rightarrow 3d^2(^3P)\ ^2P_{3/2}$	39.7188(2)	2.3(4)	1.57(5)	7.6(11)	
				XVI	39.7681(2)	7.2(3)	2.93(2)		
				XVII	40.1917(2)	$< 0.1(-)$	2.9(1)		
40.97	7.69	0.219	100.	$^2D_{5/2} \rightarrow 3d^2(^3F)\ ^2D_{5/2}$	40.1943(2)	0.9(1)	19.2(8)	35.(3)	
40.99	0.463	0.067	0.0003	$^2D_{5/2} \rightarrow 3d^2(^3F)\ ^2D_{3/2}$					
40.99	0.495	0.219	9.66	$^2D_{3/2} \rightarrow 3d^2(^3F)\ ^2D_{5/2}$	40.2190(2)	0.8(2)	1.55(6)	7.5(11)	
41.02	4.96	0.067	0.004	$^2D_{3/2} \rightarrow 3d^2(^3F)\ ^2D_{3/2}$					
				XVIII	40.2542(2)	$< 0.1(-)$	0.95(4)		
43.01	0.200	49.7	47.8	$^2S_{1/2} \rightarrow 3d(^1D)4d\ ^2P_{1/2}$					
43.01	0.870	26.0	11.0	$^2S_{1/2} \rightarrow 3d(^3F)4d\ ^2P_{3/2}$					
43.18	3.22	225.	177.	$^2S_{1/2} \rightarrow 3d(^1P)4s\ ^2P_{1/2}$ }	41.8065(3)	148.(1)	56.6(2)	229.(12)	
43.19	6.01	204.	330.	$^2S_{1/2} \rightarrow 3d(^1P)4s\ ^2P_{3/2}$					

[a] [Ne]$3s^23p^63d$ or [Ne]$3s^23p^64s$ are omitted in the initial and [Ne]$3s^23p^5$ is omitted in the final state designation.